

High-energy electrons from the muon decay in orbit: radiative corrections

Robert Szafron, Andrzej Czarnecki

*Department of Physics, University of Alberta, Edmonton,
Alberta, Canada T6G 2G7*

October 28, 2015

Abstract

We determine the $\mathcal{O}(\alpha)$ correction to the energy spectrum of electrons produced in the decay of muons bound in atoms. We focus on the high-energy end of the spectrum that constitutes a background for the muon-electron conversion and will be precisely measured by the upcoming experiments Mu2e and COMET. The correction suppresses the background by about 15%.

In matter, muons decay differently from antimuons. Although the decay rates are very similar [1], negatively charged μ^- can bind with nuclei. The nucleus exchanges photons with the muon and the daughter electron, rearranging the energy distribution. In this paper we find how this rearrangement is affected by the real radiation and self-interaction on the muon-electron line. We predict the energy spectrum of the highest-energy electrons, interesting both theoretically and experimentally.

For a theorist, the muon decay is the simplest example with which to understand the gamut of binding effects, including the motion in the initial state, interplay of the binding and the self-interaction, and the recoil of the nucleus. Experimenters have recently studied the bound muon decay (decay in orbit, DIO) [2] with a precision sufficient to probe radiative corrections, later evaluated in [3]; however, these studies concern only the lower half of the spectrum, largely accessible also to a free muon.

Interestingly, the energy range of electrons produced in the DIO reaches to about twice the maximum possible in a free muon decay. When the muon decays in vacuum, momentum conservation requires that at least half of the energy be carried away by the neutrinos. In the DIO, the nucleus can absorb the momentum without taking much energy because it is so heavy.

The high-energy part is important for the upcoming searches for the ultra-rare neutrinoless muon-electron conversion, COMET in J-PARC [4] and Mu2e in Fermilab [5]. Designed for a sensitivity better than one exotic conversion in 10^{16} ordinary muon decays, they will collect large samples of events with high-energy electrons. A reliably predicted spectrum is needed to distinguish the exotic signal – an excess of electrons at maximum energy – from the Standard Model background.

Predicting the DIO spectrum is a challenge because both the decaying muon and the daughter electron interact with the Coulomb field of the nucleus. A numerical calculation with Coulomb-Dirac wave functions is possible [6] provided that self-interactions (photons attached to the muon and the electron) are neglected. How can they be included? In the lower half of the spectrum the muon and the electron can be treated as nearly free and the binding effects can be factorized. Then the radiative corrections, known for a free muon, are convoluted with a shape function that parametrizes the Coulomb

field effect [3, 7]. Here we construct an expansion around the end-point and employ it to find radiative corrections also to the high-energy part of the spectrum.

Accounting for the external Coulomb field in charged-particle propagators is called the Furry picture [8]. In this formulation, and still ignoring radiative corrections, a single diagram, shown in Fig. 1, describes the DIO. We shall demonstrate that the bound-state radiative corrections are easiest to evaluate

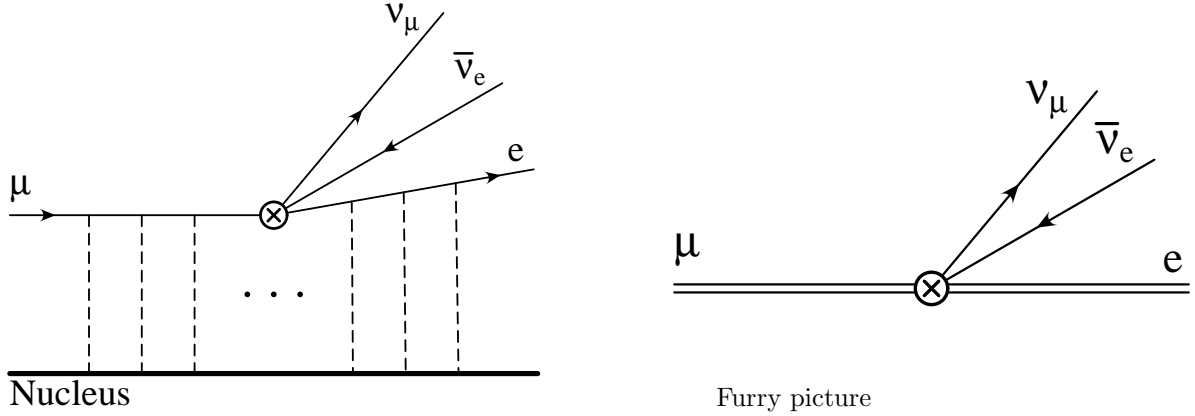


Figure 1: Muon decay in orbit (DIO). Dashed lines denote Coulomb photons exchanged between charged leptons and the nucleus. The right panel shows the same physics using double lines for charged leptons propagating in the Coulomb field.

near the high-energy end of the spectrum, the most important part for the new experiments. For now we neglect the nuclear recoil and structure, and treat the nucleus as an infinitely-heavy point source of the Coulomb field. We denote the electron energy with E ; its maximum value is $E_{\max} \simeq m_\mu \left(1 - \frac{(Z\alpha)^2}{2}\right)$, where m_μ is muon mass, Z is the atomic number, and $\alpha \simeq 1/137$ is the fine-structure constant. The DIO spectrum near its end-point can be expanded in the small parameter $\Delta = \frac{E_{\max} - E}{m_\mu}$,

$$\frac{m_\mu}{\Gamma_0} \frac{d\Gamma}{dE} = \sum_{ijk} B_{ijk} \Delta^i (\pi Z\alpha)^j \left(\frac{\alpha}{\pi}\right)^k, \quad (1)$$

where $\Gamma_0 = \frac{G_F^2 m_\mu^5}{192\pi^3}$ is the free-muon decay rate and G_F is the Fermi constant [9, 10]. Powers of $\pi Z\alpha$ parameterize photon exchanges with the nucleus and α/π arises from radiative corrections on the charged-lepton line and the vacuum polarization. The first non-vanishing term has $i = j = 5$ and $k = 0$, with $B_{550} = \frac{1024}{5\pi^6} \simeq 0.21$. Higher order coefficients B may have logarithms of $Z\alpha$ and Δ .

Corrections to this leading behavior have several sources. The large momentum transfer to the nucleus probes its interior. The finite nuclear size, already included in [6], causes the largest correction. We will comment at the end of this paper on how to include it in our formalism. The finite nuclear mass introduces a recoil effect, also evaluated in [6]. It affects the coefficients B only slightly but it shifts the end-point energy E_{\max} .

We shall exploit a theoretical similarity between the DIO and the photoelectric effect to control higher-order binding effects. They generate powers of $\pi Z\alpha$ [11, 12] rather than $Z\alpha$. Indeed, a numerical evaluation for a point nucleus with $Z = 13$ (as in aluminum, the planned target in COMET and Mu2e) finds a -21% correction, consistent with $13\pi\alpha = 0.3$. Logarithmic enhancement starts with $(\pi Z\alpha)^7 \ln(Z\alpha)$. Fortunately, these large effects, slightly suppressed by the finite nucleus size, are summed up in the numerical evaluation [6].

Finally, the most challenging corrections result from radiative effects that are the subject of this study. Before delving into the physics of the end-point, we present our main result. Close to the end-point,

including radiative corrections, the DIO spectrum for aluminum is

$$\frac{m_\mu}{\Gamma_0} \frac{d\Gamma}{dE} \approx 1.24(3) \times 10^{-4} \times \Delta^{5.023}. \quad (2)$$

To illustrate the importance of the new corrections we consider the last 150 keV of the spectrum (the typical planned resolution of Mu2e and COMET). Radiative corrections reduce the number of events in this bin by 15%, a welcome reduction of the background, comparable in size with higher-order binding effects.

In the remainder we explain the origin of such a large effect. We begin with the tree-level behaviour, appropriately expanding the lepton wave functions. We find that an exchange of a single, highly virtual photon gives the electron an energy of the full muon mass.

The relativistic electron is described by a plane wave distorted by the Coulomb potential V ; to the first order,

$$\bar{\psi}_p(\vec{q}) = \bar{u}(p) \left[\delta^3(\vec{p} - \vec{q}) + \not{V}((\vec{p} - \vec{q})^2) \frac{1}{\not{q} - m_e} \right], \quad (3)$$

where $u(p)$ is a spinor solution of a free Dirac equation and the four-potential in momentum space reads

$$V(\vec{k}^2) = \left(-\frac{Z\alpha}{2\pi^2 \vec{k}^2}, \vec{0} \right). \quad (4)$$

A muon bound to a nucleus with $Z \ll 137$ is nonrelativistic. Nevertheless, we will need the first relativistic correction to its wave function, just like in the classic analysis of the photoelectric effect [13],

$$\psi(\vec{q}) = \psi_{\text{NR}}(\vec{q}) \left(1 + \frac{\vec{q} \cdot \vec{\gamma}}{2m_\mu} \right) u(P), \quad (5)$$

where $\psi_{\text{NR}}(\vec{q}) = \frac{8\pi Z\alpha m_\mu \Psi(0)}{[\vec{q}^2 + (Z\alpha m_\mu)^2]^2}$ is the nonrelativistic momentum-space wave function of the 1S ground state with $\Psi(0) = \left(\frac{Z\alpha m_\mu}{\pi^{1/3}} \right)^{3/2}$; $u(P)$ is the four-spinor of a muon at rest, $P = (m_\mu, 0)$.

We now consider separately the contributions of the two terms in the electron wave function (3). The delta function term forces the muon momentum in (5) to be large, $\vec{q} = \vec{p} \sim m_\mu$. Thus we neglect $Z\alpha m_\mu$ in the denominator of ψ_{NR} and find

$$\psi(\vec{q}) \approx (2\pi)^3 \Psi(0) \frac{1}{\not{p} + \not{q} - m_\mu} \not{V}(\vec{q}^2) u(P). \quad (6)$$

This is visualized in Fig. 2a: the muon, before decaying, transfers momentum $\vec{q} \sim m_\mu$ to the nucleus through a hard space-like photon. It is here that the relativistic correction to the muon wave function is important.

The second term in (3) refers to an electron scattered on the nucleus. Now the muon momentum, not restricted to large values, has its typical bound-state size $\vec{q} \sim Z\alpha m_\mu$, negligible in comparison with $\vec{p} \sim m_\mu$. We use $\lim_{a \rightarrow 0} \frac{8\pi a}{(q^2 + a^2)^2} = (2\pi)^3 \delta^3(\vec{q})$ to approximate the muon wave function,

$$\psi(\vec{q}) \approx (2\pi)^3 \Psi(0) \delta^3(\vec{q}) u(P). \quad (7)$$

This is shown in Fig. 2b, where the hard photon is exchanged after the decay.

The two diagrams in Fig. 2 add up to the leading contribution B_{550} in (1). In both cases any energy unused by the electron ($\sim \Delta$) is taken up by the neutrinos and not transferred to the nucleus. Counting

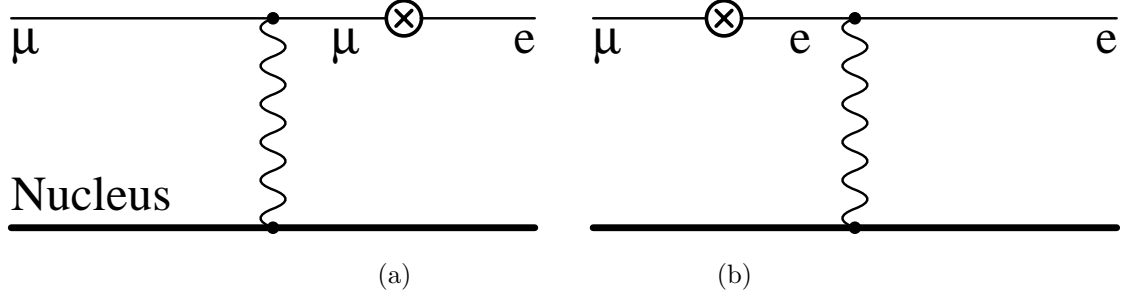


Figure 2: Furry diagram expanded in $Z\alpha$. Crossed circles indicate insertions of the weak interaction transforming the muon into an electron; the emitted neutrinos are not shown. These two amplitudes give rise to the highest-energy electrons.

neutrino momenta in the integrated matrix element explains the leading energy dependence in (1),

$$\int \frac{d^3\nu}{\nu_0} \frac{d^3\bar{\nu}_0}{\bar{\nu}_0} \delta(m_\mu\Delta - \nu_0 - \bar{\nu}_0) \dots \psi \dots \bar{\psi} \sim \Delta^5. \quad (8)$$

Having understood that only two diagrams describe the end-point behavior, we are now ready to evaluate radiative corrections. In the Furry picture there are two groups of virtual corrections, shown in Fig. 3. We expand them in $Z\alpha$ just like the tree-level diagrams, but in addition to wave functions (3, 5), we need also the Coulomb-Dirac Green's function [14],

$$\begin{aligned} -iG^V(E; \vec{p}, \vec{p}') &\simeq \frac{\delta^3(\vec{p} - \vec{p}')}{\not{p} - m} \\ &+ \frac{1}{\not{p} - m} \not{V}((\vec{p} - \vec{p}')^2) \frac{1}{\not{p}' - m}. \end{aligned} \quad (9)$$

The expansion (9) reduces radiative corrections in an external field to a set of loop diagrams that we

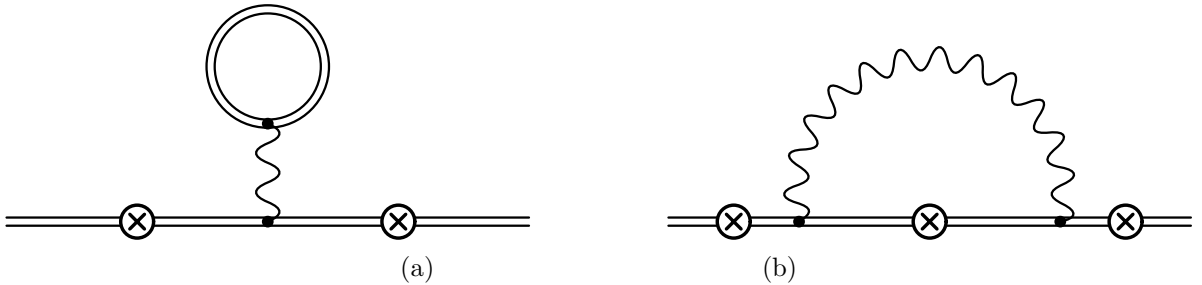


Figure 3: Virtual corrections to the muon DIO (Furry picture).

evaluate analytically [15]. This approach can be extended to higher-order corrections.

The diagram in Fig. 3a adds the Uehling correction to the Coulomb potential [16] and modifies the photon propagators in Fig. 2. In muonic aluminum the range of the Uehling potential exceeds the Bohr radius. It strengthens the attractive force and increases the muon wave function at the origin,

$$\Psi(0) \rightarrow \Psi(0) \left(1 + \frac{\alpha}{\pi} \delta_0\right). \quad (10)$$

For aluminum we find $\delta_0 = 3.27$. This correction reflects the running of the coupling α up to the average muon momentum scale $m_\mu Z\alpha$.

Vacuum polarization loops on the highly virtual photon propagators are related to the running of α

up to the hard scale m_μ . They enhance the tree-level decay rate by a factor $1 + \frac{\alpha}{\pi}\delta_{\text{VP}}$, with

$$\delta_{\text{VP}} = \frac{4}{3} \ln \frac{m_\mu}{m_e} - \frac{10}{9} + 0.12 \approx 6.1, \quad (11)$$

where the term 0.12 arises from a muon loop.

Another correction comes from the real radiation. Diagrams represented by Fig. 4 are expanded in

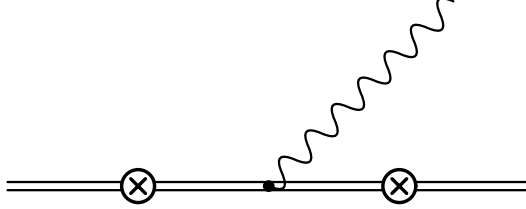


Figure 4: Furry diagram for the real radiation correction.

the same way as virtual corrections, using (9). Near the end-point the eikonal approximation suffices; by energy conservation the real photons must be soft, $0 < E_\gamma < m_\mu \Delta$.

The sum of virtual and real radiation is finite,

$$\frac{B_{551}}{B_{550}} = \delta_{\text{H}} + \delta_{\text{s}} \ln \Delta, \quad (12)$$

where the vacuum polarization corrections δ_{VP} and δ_0 are included with hard self-interaction effects in $\delta_{\text{H}} = 6.31 - \frac{26}{15} \ln \frac{m_\mu}{m_e}$, and $\delta_{\text{s}} = 2 \ln \frac{2m_\mu}{m_e} - 2$ is a soft correction. The latter can be exponentiated [17] (similarly to the free-muon decay [18]) and vanishes when $\Delta \rightarrow 0$,

$$B_{550} + \frac{\alpha}{\pi} B_{551} \rightarrow B_{550} \left(\Delta^{\frac{\alpha}{\pi} \delta_{\text{s}}} + \frac{\alpha}{\pi} \delta_{\text{H}} \right), \quad (13)$$

instead of unphysically diverging as $\ln \Delta$. It increases the exponent of Δ and suppresses DIO events near the end-point. The relative decrease is inversely correlated with the energy resolution: the number of electrons in the end-point bin of 1 (0.1) MeV is reduced by 11% (16%).

The final-state electron is relativistic, $E \gg m_e$, so its structure function [19, 20] is insensitive to Coulomb corrections. A convolution with the free-decay spectrum confirms the coefficient $-\frac{46\alpha}{15\pi}$ of $\ln \frac{m_\mu}{m_e}$ due to collinear photons. Together with the vacuum polarization in (11), this explains the logarithmic part of the hard correction.

That log is largely cancelled in the sum with the wave function correction in (10) and $\delta_{\text{H}} = -2.9$ reduces the end-region by only a fraction of a per cent. We thus neglect the unknown hard corrections $\mathcal{O}((\alpha/\pi)^2)$ in the error estimate, dominated by the nuclear-size effects, discussed below.

There are now two complementary studies of the end-point spectrum. Here, we have computed radiative corrections (RC) assuming a point nucleus and considering only the one-Coulomb exchange. Ref. [6] did not have the RC but included the nucleus structure, recoil, and multiple Coulomb interactions.

In order to combine these results, we observe that the most important – soft – correction is universal, not sensitive to any interactions with the nucleus. The hard correction is tiny, so treating it also as universal is well within our final error estimate.

In the discussion of the uncertainty we specialize to aluminum but the discussion can be applied to other nuclei, so we keep the Z dependence explicit. We assume a Fermi charge distribution,

$$\varrho = \frac{\rho_0}{1 + \exp \frac{r-r_0}{a_0}} \quad (14)$$

with $a_0 = 0.569$ fm and $r_0 = 2.84(5)$ fm [21].

The finite size affects the nucleus form-factor, defined as a ratio of Fourier transforms of potentials from the extended (14) and the point-like (4) charge distributions,

$$F_\rho(\vec{k}^2) = \frac{V_\rho(\vec{k}^2)}{V(\vec{k}^2)} \longrightarrow 0.64 \quad \text{for } \vec{k}^2 = m_\mu^2. \quad (15)$$

The DIO spectrum for a finite nucleus has an expansion analogous to (1), but with coefficients that depend on the density ρ . Its leading term near the end-point [6] is

$$\sum_{j=5}^{\infty} B_{5j0}^\rho [F_\rho(m_\mu^2) \pi Z \alpha]^j = 8.98 \times 10^{-17} \left(\frac{m_\mu}{\text{MeV}} \right)^6. \quad (16)$$

This result includes exchanges of many Coulomb photons, in addition to the single hard exchange to which we have found the radiative correction. We estimate the magnitude of the multi-Coulomb part as a fraction $f = F_\rho(m_\mu^2) \pi Z \alpha \simeq 0.2$ of (16).

Hard radiative corrections to this part are missing. To be conservative, we are not assuming that they involve a cancellation that has suppressed δ_H . Corrections on the order of the collinear logarithm translate into a relative error of about $\frac{46\alpha}{15\pi} f \ln \frac{m_\mu}{m_e} \simeq 0.7\%$. In addition, experimental errors in the charge distribution parameters (14) introduce a 2% uncertainty [6]. Summing them in quadrature, together with the sensitivity to the scale involved in the exponentiation of soft effects, we arrive at an error around 2.5% in the end-point spectrum.

The result (16), multiplied by the new correction (13), leads to our prediction for the end-point spectrum, (2).

To summarize, we have determined the correction to the high-energy tail of the DIO energy distribution and its remaining uncertainty. Key to this improvement has been the simplicity of the leading amplitudes that turn out to arise from a small number of hard-photon exchanges. This line of reasoning can be extended to higher-order binding effects, at least for a point nucleus. For a realistic charge distribution, a numerical evaluation of loop diagrams will be necessary. However, the leading radiative correction has now been established with good precision. Its sizeable negative effect on the DIO will make any observed event near the end-point an even more convincing signal of New Physics, a discovery we eagerly anticipate.

This research was supported by Natural Sciences and Engineering Research Council (NSERC) of Canada. R.S. acknowledges support by the Polish National Science Centre (NCN) under Grant Agreement No. DEC-2013/11/B/ST2/04023 and by the Fermilab Intensity Frontier Fellowship. Fermilab is operated by Fermi Research Alliance, LLC under Contract No. De-AC02-07CH11359 with the United States Department of Energy.

References

- [1] A. Czarnecki, G. P. Lepage, W. J. Marciano, Muonium Decay, Phys. Rev. D61 (2000) 73001.
- [2] A. Grossheim et al., Decay of Negative Muons Bound in Aluminum, Phys. Rev. D80 (2009) 052012.
- [3] A. Czarnecki, M. Dowling, X. Garcia i Tormo, W. J. Marciano, R. Szafron, Michel Decay Spectrum for a Muon Bound to a Nucleus, Phys. Rev. D90 (2014) 093002.
- [4] Y. Kuno, A Search for Muon-To-Electron Conversion at J-PARC: the COMET Experiment, PTEP 2013 (2013) 022C01.

- [5] D. Brown, Mu2E, a Coherent $\mu \rightarrow e$ Conversion Experiment at Fermilab, AIP Conf. Proc. 1441 (2012) 596.
- [6] A. Czarnecki, X. Garcia i Tormo, W. J. Marciano, Muon Decay in Orbit: Spectrum of High-Energy Electrons, Phys. Rev. D84 (2011) 013006.
- [7] R. Szafron, A. Czarnecki, Shape Function in QED and Bound Muon Decays, Phys. Rev. D92 (5) (2015) 053004.
- [8] W. Furry, On Bound States and Scattering in Positron Theory, Phys. Rev. 81 (1951) 115.
- [9] D. Webber et al., Measurement of the Positive Muon Lifetime and Determination of the Fermi Constant to Part-per-Million Precision, Phys. Rev. Lett. 106 (2011) 041803.
- [10] W. J. Marciano, Fermi Constants and “New Physics”, Phys. Rev. D60 (1999) 093006.
- [11] R. Pratt, A. Ron, H. Tseng, Atomic Photoelectric Effect Above 10 keV, Rev. Mod. Phys. 45 (1973) 273.
- [12] J. Eichler, T. Stöhlker, Radiative Electron Capture in Relativistic Ion–Atom Collisions and the Photoelectric Effect in Hydrogen-like High-Z Systems, Phys. Rep. 439 (2007) 1.
- [13] V. B. Berestetsky, E. M. Lifshitz, L. P. Pitaevsky, Quantum Electrodynamics, Pergamon Press, Oxford, 1982.
- [14] J. Schwinger, Particles, Sources and Fields, Vol. 2, Addison-Wesley, Redwood City, CA, 1973.
- [15] A. V. Smirnov, FIRE5: a C++ Implementation of Feynman Integral Reduction, Comput. Phys. Commun. 189 (2014) 182.
- [16] E. A. Uehling, Polarization Effects in the Positron Theory, Phys. Rev. 48 (1935) 55.
- [17] D. R. Yennie, S. C. Frautschi, H. Suura, The Infrared Divergence Phenomena And High-Energy Processes, Ann. Phys. 13 (1961) 379.
- [18] W. J. Marciano, G. C. Marques, N. Papanicolaou, On Infrared Problems in Muon Decay, Nucl. Phys. B96 (1975) 237.
- [19] A. Arbuzov, A. Czarnecki, A. Gaponenko, Muon Decay Spectrum: Leading Logarithmic Approximation, Phys.Rev. D65 (2002) 113006.
- [20] A. Arbuzov, K. Melnikov, $O(\alpha^2) \ln(m_\mu/m_e)$ Corrections to Electron Energy Spectrum in Muon Decay, Phys.Rev. D66 (2002) 093003.
- [21] H. De Vries et al., Nuclear Charge-Density-Distribution Parameters From Elastic Electron Scattering, At. Data and Nucl. Data Tables 36 (1987) 495.